Meta-Gaps for Mechanically Reconfigurable Phased Arrays

D. Elliott Williams[#1] and Ali Hajimiri[#]

[#]Caltech Holistic Integrated Circuits Lab, Caltech, Pasadena, CA 91125, USA

[1]elliott@caltech.edu

***Abstract* — Meta-material inspired switched passive networks on flexible sheets can be placed in the unused area between antennas in Origami and Kirigami shape-changing arrays. These *meta-gaps* can manipulate the near-field environment in order to compensate for the increased spacing in these arrays. Their flexibility allows meta-gaps to easily fold and deploy in both deployable arrays and mechanically shape-changing phased arrays. This work explores the promise of meta-gaps through the measurement of a 5-by-5 element λ-spaced array with 40 meta-gap sheets and 960 switches. The complexity of optimizing such a high-dimensional system is discussed and solutions are proposed. Measurement results demonstrate that in our implementation, meta-gaps increase the broadside main beam power by 0.9 dB, suppress the sidelobes by 4.6 dB, and enhance the field-of-view by 23° compared to a ground plane.**

***Keywords* — phased arrays, adaptive arrays, metamaterials, flexible electronics, origami antennas, kirigami antennas, measurement techniques, optimization, metaheuristics, simulated annealing, genetic algorithms, particle swarm optimization**

I. Introduction

The recent development of mechanically shape-changing phased arrays shows the promise of using geometric reconfiguration to optimize for a given array behavior [1]. However, Gauss's *Theorema Egregium* requires that the surface area of an array must stretch or contract as it changes between shapes with different Gauss curvature [2]. If the number of radiators in an array is fixed, the spacing between them must change as the array shifts between planar and spherical shapes. Thus, Origami- and Kirigami-based arrays of rigid tiles can only change shape if *gaps* are introduced between the tiles.

This increased element spacing will alter array performance by reducing the fill factor, introducing grating lobes, and altering the antenna coupling. But these gaps also present an opportunity in the form of extra unused area on the radiation surface that can be filled with switch-controlled flexible passive structures capable of distorting the near-field environment. Such meta-surface inspired structures, henceforth referred to as *meta-gaps*, can be used to mitigate the effects of increased element spacing. Similar mechanisms have been used to create a programmable reflectarray [3], to reconfigure antenna geometry [4], and to modulate the radiation pattern for physically secure wireless communication [5].

Figure 1 illustrates the advantages of *flexible* meta-gaps. In a planar shape there are no gaps, so the meta-gaps fold behind ground plane backed antennas where they will minimally interact with the radiating surface. When the array changes into a cylinder, the meta-gaps are deployed between the antennas and are configured to mitigate the effects of increased antenna spacing or otherwise enhance the array performance.

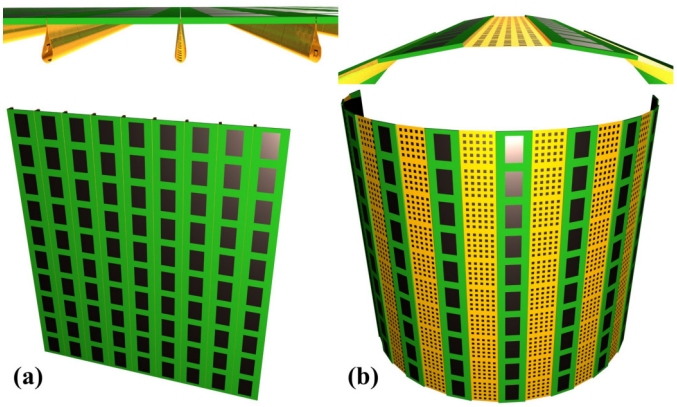

Fig. 1. Illustration of how meta-gaps can be deployed to fill the gaps in a shape-changing array. (a) In planar configuration the sheets fold behind the tiles. (b) In cylindrical configuration they expand to fill the gaps.

This work explores the promise of flexible meta-gaps by incorporating them into a planar $\lambda-$spaced 2D array and using *in-situ* optimization to study the effect of switch settings on the grating lobes. Section II presents the design of the array and meta-gap sheets. Section III discusses the measurement approach used for rapid array characterization. Section IV details the optimization problem and algorithmic approach and Section V presents and analyzes measurement results.

II. Array Design

The presented meta-gap array shown in Figure 2 consists of 25 independent radiating tiles separated by 40 meta-gap sheets, each containing 24 RF switches. The λ-spaced array operates at 2.5 GHz with 6 cm tiles and meta-gap sheets.

A. Tile Design

Each tile is a 2.5 GHz radiator with programmable phase and amplitude. The tiles' RF outputs are synchronized by locking to a 78.125 MHz reference. The signal is radiated by a patch antenna on the opposite side of the tile. The patch ground plane isolates the radiator from the electronics. Figure 2 shows both sides of the tile and the measured and FEM-simulated radiation patterns. The simulated antenna efficiency is 84%.

Each tile also serves as a controller for two neighboring meta-gaps using programmable headers. Power, programming, and reference signals are distributed through the array using a

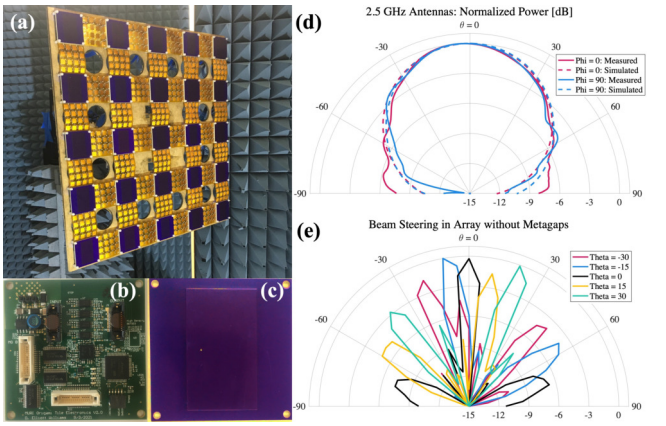

Fig. 2. (a) Array with Meta-gaps. Tile (b) front and (c) backside. (d) Single tile element pattern. (e) Measured beam patterns of array without meta-gaps.

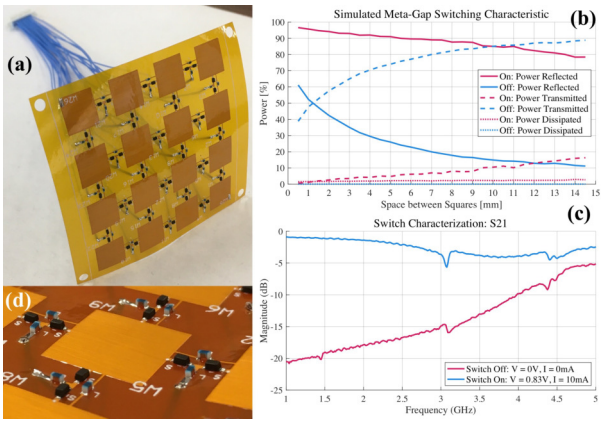

Fig. 3. (a) Meta-gap sheet. (b) Simulation of reflectivity and transparency versus gap size. (c) Measured switch S_{21}. (d) Close-up of switches.

single cable. To reduce the total current carried by the cables, power is distributed at 30V and down-converted to 3.3V by a local DC-to-DC converter on each tile.

B. Meta-gap Design

The meta-gap sheet shown in Figure 3 is comprised of a 0.5-oz copper layer between two 1-mil layers of flexible polyimide. The metal forms a 4-by-4 grid of 9.7mm squares with 5.3mm gaps. Neighboring squares are connected by an RF switch consisting of a pair of series PIN diodes biased with a 30 nH RF choke inductor. The measured switching behavior of the structure is shown in Figure 3. A common DC ground is established by using 30 nH inductors to connect adjacent squares. Each switch is controlled with a 10 mA current via a header containing 24 control wires and 2 ground wires. The lightweight 32 AWG wires are connected to the sheet from the back side in order to maximize sheet flexibility and minimize unwanted near-field interactions.

The meta-gaps are designed to achieve maximum variation in reflectivity and transparency when all switches are simultaneously turned on and off. When all the switches are on, the surface ideally behaves like a ground plane, maximizing the reflection of incident waves. When all the switches are off, the surface ideally is transparent to incident waves. An FEM analysis characterizing the relationship between metal spacing and the surface's ability to reflect incident plane waves is shown in Figure 3. A space size of 5.3mm is selected to minimize the power reflected in the off state while reflecting 90%, and only dissipating 5.4%, of the power in the on state.

III. Array Characterization and Measurement

Completely characterizing the performance of a phased array requires a large number of measurements. A full 3D radiation pattern must be measured for every beam angle within the steering range in order to get a *complete* picture of the power radiated in both the desired (main beam) and undesired (side lobe) directions. Managing this measurement complexity is critical for characterizing meta-gaps because each switch configuration effectively creates a new array that requires complete characterization.

A. Array Figures of Merit

In order to reduce the number of measurements used for characterization, we evaluate the performance of the array by the power radiated in the main beam direction (MBP), the side lobe level (SLL), and the field of view (FoV) in the E- and H-plane cuts. SLL is here defined as the relative strength of the peak side lobe with respect to the MBP and FoV is defined as the range over which the SLL is negative. These measures provide insight into the array's maximum EIRP, 3-dB steering range, and gain, without requiring a full 3D scan. Beams are only steered within the FoV when characterizing the MBP and SLL because, due to spatial aliasing, the phase settings required to steer a beam outside of the FoV are the same as those that steer a beam at a different angle *inside* of the FoV. Since the beam strength is higher within the FoV, the beam on the outside is not truly the main beam, but a grating lobe of the beam on the inside. The FoV of an ideal λ- spaced array is $\pm 30^{\circ}$, greatly reducing the number of measurements.

B. Array Characterization Time

An efficient measurement approach is necessary to perform *in-situ* optimization. The average time to move the antenna under test or a probe between measurement points, T_{move}, in a radiation pattern measurement is on the order of seconds, while the measurement time, T_{meas}, can theoretically be less than a microsecond. Assuming $T_{meas} \ll T_{move}$, the time to characterize a phased array is:

$$T_{char} \approx N_b(N_m + 1)T_{move} \quad (1)$$

where N_m is the number of measurement points per beam and N_b is the number of beams used to characterize the array.

Equation 1 is the fixed time required to move between all the measurement points. If T_{move} is one second, then it takes 90 minutes to characterize *a single meta-gap configuration* along two cuts with 5° precision. If M states are measured sequentially than the total measurement time is MT_{char}.

Instead, multiple configurations can be measured in parallel by iterating through them at each measurement point. Thus a large number of configurations can be characterized while only

moving through measurement points once. In this case the time to characterize a batch of M configurations is:

$$T_{batch} \approx T_{char} + MN_bN_m[(N_{tiles} - 1)D + 1]T_{meas} \quad (2)$$

where N_{tiles} is the number of tiles and D is the number of measurements required to optimize the beam phase settings.

For a sufficiently large batch size the total characterization time is decreased by orders of magnitude. However, results are not available until the entire batch is processed. Thus algorithms must operate on batches of measurements, as no decision can be made until the completion of each batch.

IV. Optimization

A. Problem Scalability and Structure

Meta-gaps present a high-dimensional configuration space with a far smaller subspace of useful solutions; a meta-gap structure with k switches has 2^k possible states. Finding optimal switch states for this kind of switching network has been proven to be NP-Hard in general and there is no known convex heuristic that consistently identifies good solutions [6].

Thus, non-convex heuristic algorithms must be employed in order to identify preferred, if not optimal configurations. While problem-specific heuristics will outperform abstract metaheuristic algorithms [7], it is not obvious how a given set of switches will alter the array behavior due to the strongly non-linear behavior of switched networks and the complex interactions of parasitic elements in response to different electromagnetic excitations for different steering angles.

Four different metaheuristic algorithms and a simple random search are employed to both explore meta-gap performance and to provide insight into the general structure of the optimization problem and its solutions. The selected algorithms -Genetic, Variable Neighborhood Search (VNS), Particle Swarm (PS), and Simulated Annealing (SA)- take advantage of different properties of the optimization problem, while the random search serves as a baseline comparison. Thus properties of the problem structure can be identified by comparing the relative performance of these methods.

While the total array has 960 switches, in this analysis each meta-gap sheet is restricted to have the same switch settings in order to restrict the size of the search space to 24 bits and increase the effect each bit has on the array characterization.

B. Optimization Technique

Using an automated range measurement system, each algorithm is used to optimize the array's MBP, SLL, and FoV. The algorithms operate in batches of 24 states so that search based approaches, like VNS and SA, can evaluate every neighboring state in a single batch. The algorithms are iterated for 30 batches, thus exploring a total of 720 states.

For MBP and SLL optimization, the array is measured by steering beams every 5° from -30° to 30° in the E- and H-plane cuts, while beams are steered every 5° from -90° to 90° for the FoV optimization. Beams are steered by optimizing the tile phases to maximize power in the beam direction. For all criteria, each beam pattern is measured every 5° from -90°

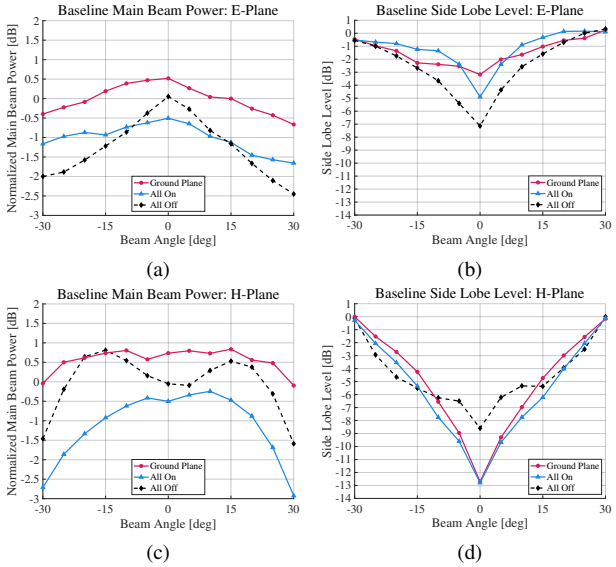

Fig. 4. Baseline measurements of Main Beam Power (a),(c) and Side Lobe Level (b),(d) in E- and H- planes for all off, all on, and ground plane baselines.

to 90° in the E- and H-plane cuts. MBP and SLL optimizations take approximately 23 hours while FoV optimizations take 60.

To compensate for low frequency noise and thermal drift over the measurement period, each batch measures a baseline state, in which every switch is turned off, and uses it to normalize the other patterns. Figure 4 shows MBP and SLL measurements for this "all off" baseline, an "all on" baseline, and with a copper ground plane placed in the gaps of the array.

V. Results

Figure 5 shows both the algorithms' performance over time and the optimal array characteristics for each of the three optimization criteria. Compared to the baseline, the meta-gaps are able to increase the MBP by over 1 dB and suppress sidelobes by more than 1.5 dB over the field of view. Broadside the performance is even better, with 1.5 dB increase in MBP and up to 4 dB supression of SLL. In addition, the meta-gaps are able to increase the array's Field of View by 23° above the theoretical value. Comparing the optimal states to the ground plane measurements in Figure 4 shows promise as meta-gaps enhance the broadside MBP by 0.9 dB and suppress the SLL by 4.6 dB. Given the limited search space and the identical sheet restrictions, meta-gaps could offer greater improvement.

This relative performance suggests that the problem has many sparsely spaced local minima in a relatively gradual global basin. VNS takes a local approach, performing a greedy search and then expanding its search space once it reaches a local optimum. Because VNS quickly identifies a decent solution and then plateaus, it is likely that local minima are relatively shallow and far apart. SA and PS have the opposite strategy, covering a wide range of spaces initially before converging locally. These algorithms both gradually approach an optimum, indicating that there is some sort of global basin. The existence of this global basin is supported by the fact that a random search is able to quickly identify a decent solution, despite random states on average being worse than

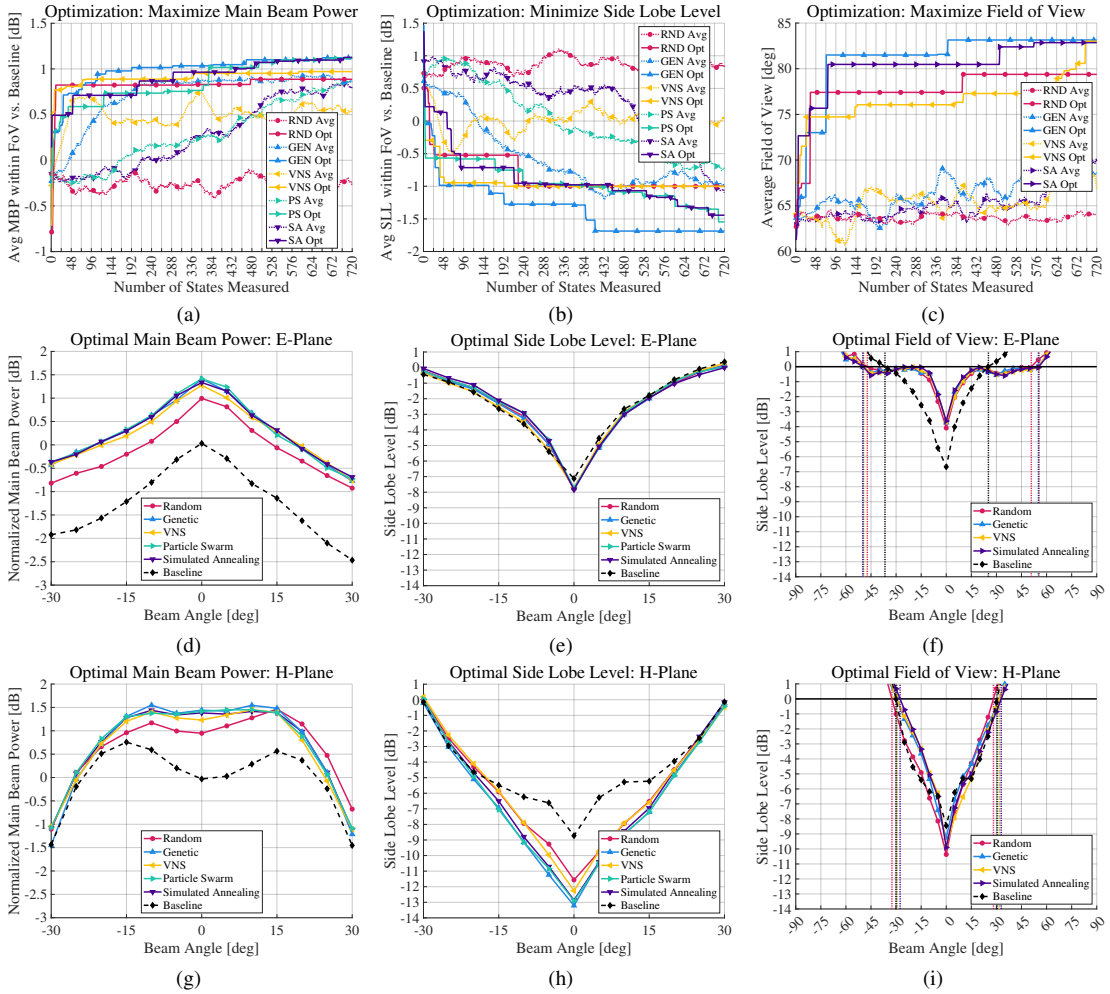

Fig. 5. Optimization curves (a)-(c) and E- (d)-(f) and H- (g)-(i) plane cuts of the optimal array characteristics for random, genetic, variable neighborhood search, particle swarm, and simulated annealing algorithms' optimization of main beam power, side lobe levels, and field of view. Optimization plots include the optimal state in addition to the value of the explored states averaged over two batches.

the baseline. Finally, the improved performance of the genetic algorithm over the other approaches suggests that problem solutions are comprised of features with intrinsic value.

These results match intuition about the electromagnetic problem. Certain patterns of conductors, like closed loops or lines of a specific length, will have a pronounced effect on the electromagnetic fields. Randomly turning switches on in general should decrease performance as switches absorb power. Changing a small number of switches can make some improvement as the state resembles a particular pattern, but many switches have to change to switch between patterns. It seems likely that there exists a smaller set of basis solutions that could greatly reduce the search space.

VI. Conclusion

This paper presents the design of a $\lambda-$spaced 2D array with programmable meta-gaps between radiators. The platform is used to explore the ability of meta-gaps to alter the array characteristics. Measurement results demonstrate that meta-gaps can enhance the main beam power, side lobe levels, and field of view of a sparse array. The comparative performance of algorithms suggests that switched passive networks are good candidates for feature based optimization, such as genetic algorithms and machine learning.

Acknowledgment

The authors thank A. Fikes, C. Ives, O. Mizrahi, and S. Nooshabadi for their help. This work was supported in part by the MURI Grant FA9550-16-1-0566 via AFOSR.

References

[1] D. E. Williams *et al.*, "Origami-inspired shape-changing phased array," in *2020 50th European Microwave Conference (EuMC)*, 2021, pp. 344–347.
[2] A. Pressley, *Elementary Differential Geometry*. London: Springer, 2010.
[3] D. Sievenpiper *et al.*, "2d beam steering using an elec. tunable imp. surface," *IEEE Trans. Ant. Prop.*, vol. 51, no. 10, pp. 2713–2722, 2003.
[4] G. Besoli *et al.*, "A multifunc. reconfig. pixeled ant. using mems tech. on pcb," *IEEE Trans. Ant. Prop.*, vol. 59, no. 12, pp. 4413–4424, 2011.
[5] A. Babakhani *et al.*, "Transmitter arch. based on near-field direct ant. mod." *IEEE J. Solid-State Circ.*, vol. 43, no. 12, pp. 2674–2692, 2008.
[6] J. Lavaei *et al.*, "Solving large-scale hybrid circuit-antenna problems," *IEEE Trans. Circ. Syst. I, Reg. Papers*, vol. 58, no. 2, pp. 374–387, 2011.
[7] D. Wolpert and W. Macready, "No free lunch theorems for optimization," *IEEE Trans on Evolutionary Computation*, vol. 1, pp. 67–82, 4 1997.